Supporting Information

Negative and positive persistent photoconductance in graphene

Chandan Biswas,[†] Fethullah Güneş,[†] Duong Dinh Loc,[†] Seong Chu Lim,[†] Mun Seok Jeong,[‡] Didier Pribat,[†] Young Hee Lee*,[†]

[†]SKKU Advanced Institute of Nanotechnology, WCU Department of Energy Science, Department of Physics, Graphene Center, Sungkyunkwan University, Suwon 440-746, Republic of Korea.

[‡]Advanced Photonics Research Institute, Gwangju Institute of Science and Technology, Gwangju 500-712, Republic of Korea.

Materials, methods and discussions:

1. Graphene synthesis

Large area monolayer graphene films were synthesized on a Cu foil by chemical vapor deposition (CVD) method. The sheet resistance and transmittance of the monolayer graphene transferred on polyethylene-terephthalate (PET) substrate was found as 725 ohm/sq and 97.6% (at 550 nm), respectively. Cu foil of 85 x 75 cm^2 with a thickness of 70 µm was rolled into a vacuum CVD quartz chamber. Temperature was increased up to 950 ^{O}C in H_2 atmosphere and annealed for an hour at this temperature prior to growth. Graphene synthesized at 950 ^{O}C by a gas flow of H_2/CH_4 : 80/250 sccm for 20 min and then the chamber was cooled down to room

temperature in the same atmosphere. After synthesis, graphene/Cu substrate was cut into equal small pieces and poly(methyl methacrylate) (PMMA) polymer (MicroChem, 950,000 MW, 2-7 wt % in chlorobenzene) was spin-casted on the graphene/Cu substrate. Copper substrate was etched by a copper etchant ($FeCl_3$) solution (type CE-100, Transene Comp. Inc.). When Cu was completely etched away, the graphene sheet with PMMA was rinsed in deionized water several times to wash away etchant residues. Subsequently, graphene/PMMA layer was floated in water to transfer on top of the prepared gold electrodes. Source and drain electrodes were prepared by gold deposition (e-beam evaporation) on a glass substrate. The channel length between two electrodes was 1 mm, while the channel width and thickness of the gold electrodes were maintained to be 1 cm each. Graphene/PMMA layer (2 x 1 cm^2) was transferred on top of the electrodes, contacting graphene to the gold electrodes (Figure 2A), while suspending graphene layers between channels. Transparent, insulating PMMA layer was used as a holding material for mechanical stability of graphene layers. Electrodes are connected to a source-measure unit (Keithley 6487) in ambient condition. In a different case, a single layer graphene was transferred on a SiO_2/Si substrate followed by gold electrode fabrication on top of it. These devices were placed at the focal length of a monochromator (Princeton Instruments, SpectraPro-150) covering whole graphene channel area by the irradiated monochromatic beam.

2. Characterizations of the graphene layers

The conductance of the samples was measured by a source-measure unit (Keithley 6487) under ambient conditions. A monochromator (Princeton Instruments, SpectraPro-150) was used to illuminate the device. UV-vis-NIR absorption spectroscopy (Varian, Cary 5000) and Raman spectroscopy (Renishaw, RM-1000 Invia) with an excitation energy of 2.41 eV (514 nm, Ar+ ion

laser) were used for characterizing the optical properties of the graphene films on PET and SiO$_2$/Si substrates. X-ray diffraction pattern (powder XRD) (D8 FOCUS 2.2 KW, Bruker AXS) with a Cu anode (1.54 Å) was used to measure the inter-layer distance of the stacked graphene layers. X-ray photoelectron spectroscopy (XPS) (QUANTUM 2000, Physical electronics, USA) was performed using a focused monochromatized Al Kα radiation (1486.6 eV).
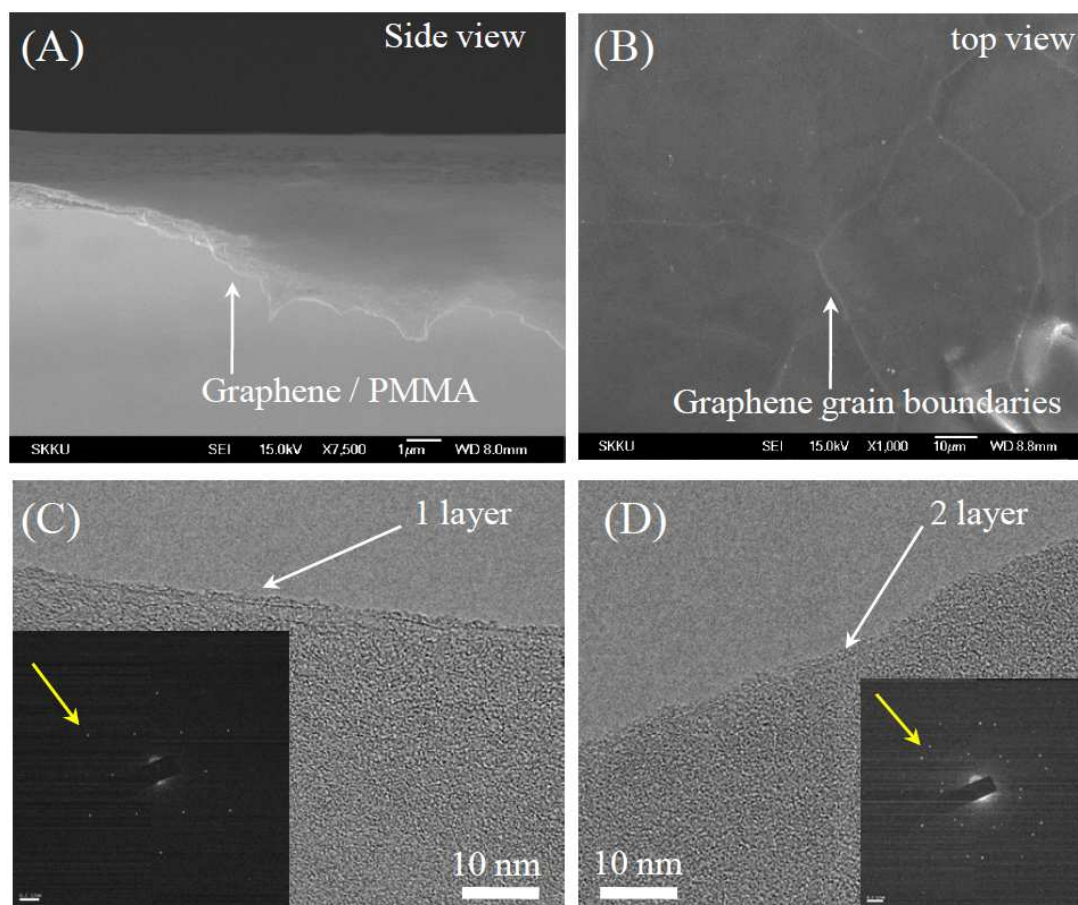

Figure S1 | **(A, B)** SEM micrographs (A, cross-sectional and, B, top view) of graphene/PMMA layer. **(C)**, HR-TEM image of monolayer graphene (white arrow) with a folded edge. The inset shows the Electron diffraction pattern from nearly normal incidence on the layer. **(D)** HR-TEM image of double layer graphene folded edge. Figure inset shows electron diffraction pattern from nearly normal incidence on double layer graphene.

Figure S1A shows the field-emission scanning electron microscope (SEM) cross section image of the graphene/PMMA sample. Cu grain boundary trace on graphene were observed in Fig. 1SB. Evidence of monolayer graphene was found in high resolution transmission electron microscope (HR-TEM) image with a single graphene edge (white arrow in Fig. S1C). Figure inset clearly shows the electron diffraction pattern from a monolayer graphene, revealing clear hexagonal symmetry. Two layers of graphene edges were visible in double layer graphene (Fig. S1D). Corresponding electron diffraction pattern shows slightly mis-oriented hexagons, revealing disordered stacking of two graphene layers.
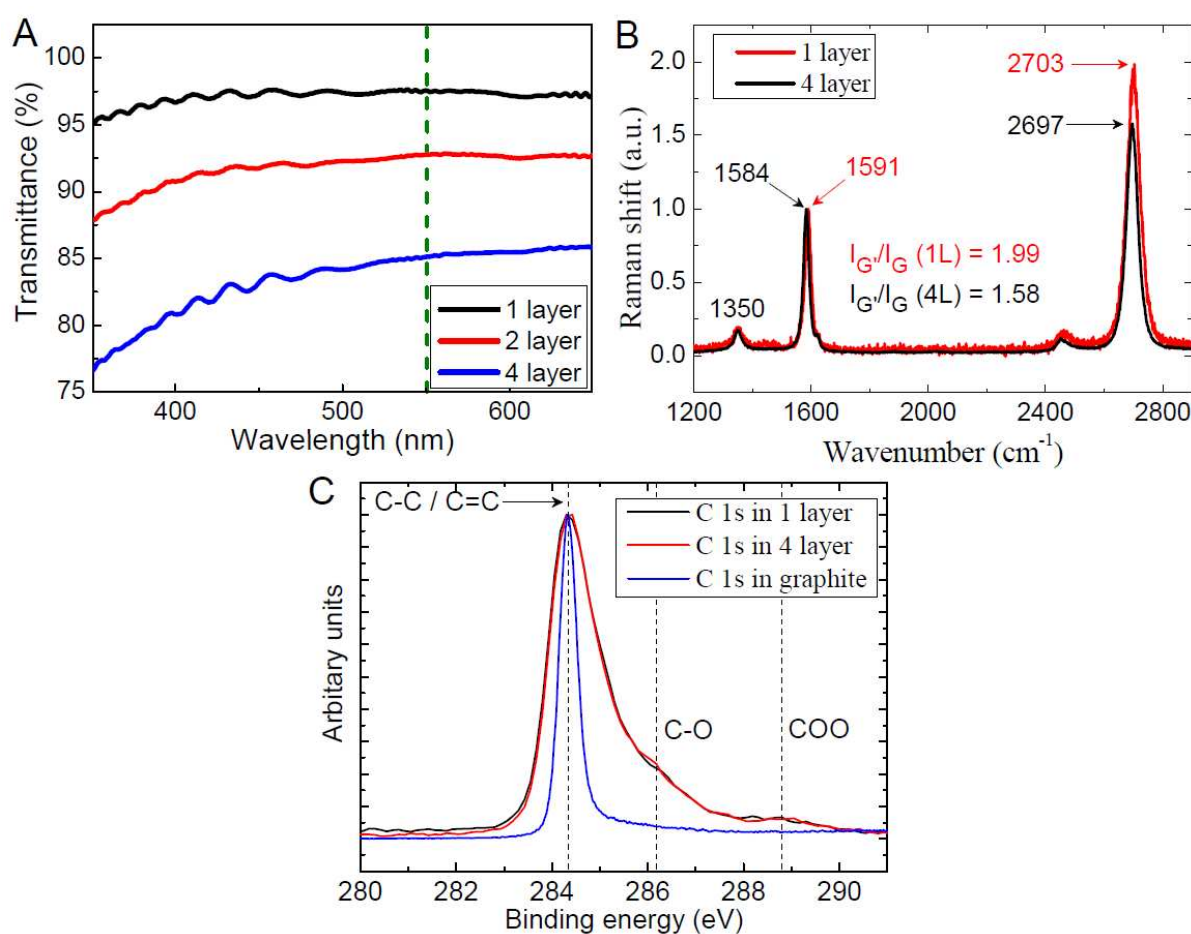

Figure S2 I **(A)** Transmittance of monolayer, double layer, and four layer graphene transferred onto PET films. **(B)** Raman spectroscopy of monolayer and four layer graphene films transferred

onto SiO$_2$ substrate. **(C)** XPS data of monolayer and four layer graphene films transferred onto PET substrate.

Graphene layers were further characterized by absorption spectroscopy, Raman spectroscopy, XRD, and XPS. Transmittance of monolayer, double layer, and four layer graphene exhibit 97.6%, 92.8%, and 85.1% transmittance, respectively at 550 nm wavelength (Fig. S2A), in consistent with the previous report of 2.3% reduction each layer (*S1*). Slight discrepancy from the double layer resulted from the residual PMMA and possibly multiple reflections. The peak positions of G-band and G'-band of the monolayer graphene were downshifted in four layer graphene and furthermore the intensity ratio of G'/G was reduced in the four layer (Fig. 2SB). This is in good contrast with the multilayer effects of HOPG samples (*S2*). This discrepancy may originate from the random stacking of the graphene layers. C-C or C=C bond has been observed in XPS analysis. The presence of C-O and COO bonds found to be existed dominantly among other absorbents (Fig. S2C) in graphene samples.

3. NPC behavior in multilayer of suspended graphene films

Figure S3A shows dynamic current measurements (*I-t*) under different illuminated light wavelengths (λ) in a single layer suspended graphene sample (sample i). Among all other illuminated wavelengths, 260 nm light excitation produces highest NPC yield, Y$_{NPC}$ (*NPC$_{max}$*) in type of graphene devices (Fig. S3B). Dark conductivity in multilayered graphene layers show higher values than single layer graphene due to multilayer stacking of graphene films. Corresponding *I-t*, and *G-λ* plots for double layer (sample ii) and four layer (sample iii) graphene presented from Fig. S3C to Fig. S3F respectively. Significantly, double and four layer graphene also shows *NPC$_{max}$* at 260 nm photon excitation confirming the M point band edge absorption in
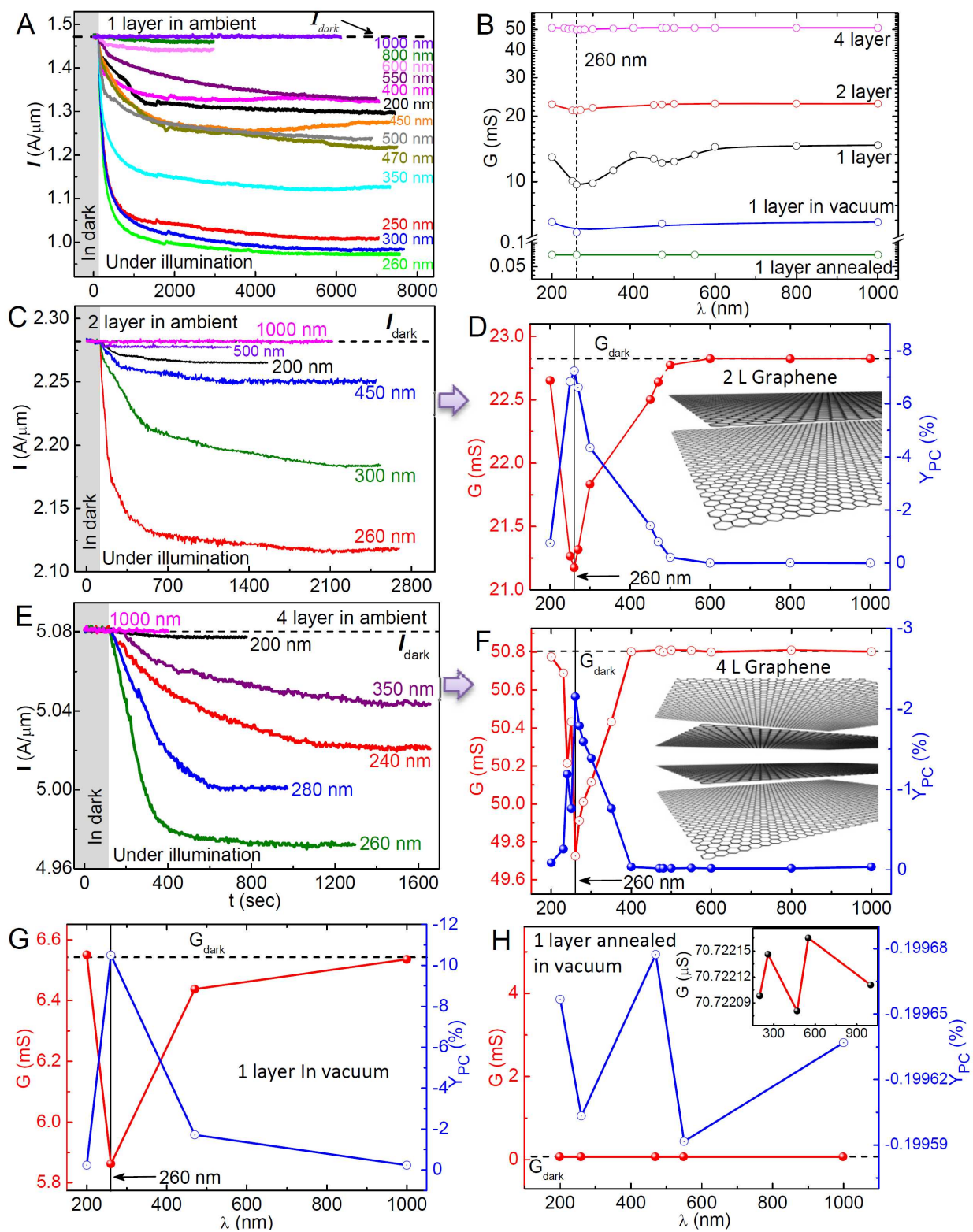
Figure S3 | (A) Dynamic current measurements (10 mV bias used for all the measurements) in monolayer of suspended graphene at different wavelengths of light irradiations. **(B)** Measured

conductance G at different wavelengths of light irradiations on monolayer (i), double layers (ii), four layers (iii), monolayer under vacuum (iv), monolayer annealed and measured under vacuum (v) samples. **(C)** I-t measurements under different wavelengths of light irradiations in sample (ii). **(D)** Measured G, and NPC yield (Y_{PC}) at different wavelength in sample (ii). **(E)** I-t measurements under different light wavelengths irradiations in sample (iii). **(F)** Measured G, and Y_{PC} values at different wavelength in sample (iii). **(G)** Measured G, and Y_{PC} values at different wavelength in sample (iv). **(H)** Measured G, and Y_{PC} values at different wavelength in sample (v). Inset shows the magnified conductance containing very small fluctuations.

graphene. Conclusively, this evidence indicates that the NPC behavior in graphene caused by the M point band edge absorption not by the plasmon resonance (π-mode) between irradiated photons and graphene. Fig. S3G and Fig. S3H shows the G-λ plots of single layer suspended graphene measured in vacuum (sample iv) and single layer suspended graphene annealed and measured in vacuum (sample v) respectively. All the samples showed NPC behavior except sample v due to oxygen/hydroxyl absorbents removal during heat treatment under vacuum. Single layer graphene shows highest Y_{NPC} (34%) where as the NPC behavior was significantly reduced in double (7%) and four layer (2%) graphene case (Fig 3B). However, NPC_{max} still existed at 260 nm in all samples except sample v (absence of NPC).

4. Current dynamics during NPC in suspended graphene

Figure S4A shows the microscopic optical image (side view) of the suspended graphene device. The graphene/PMMA layer and electrodes are marked as dotted line and solid yellow line respectively in the figure. Figure S4B is the optical image (top view) of the suspended graphene/PMMA layer near the source electrode. Copper grain boundary traces on graphene also observed in this case. Figure S4C shows the persistent nature of NPC behavior in sample (i) at 500 nm irradiation. Current value decreases upon light irradiation and saturates after long time (t_{sat}) (nearly 2 hr). The inset of the figure shows a magnified view during saturation.
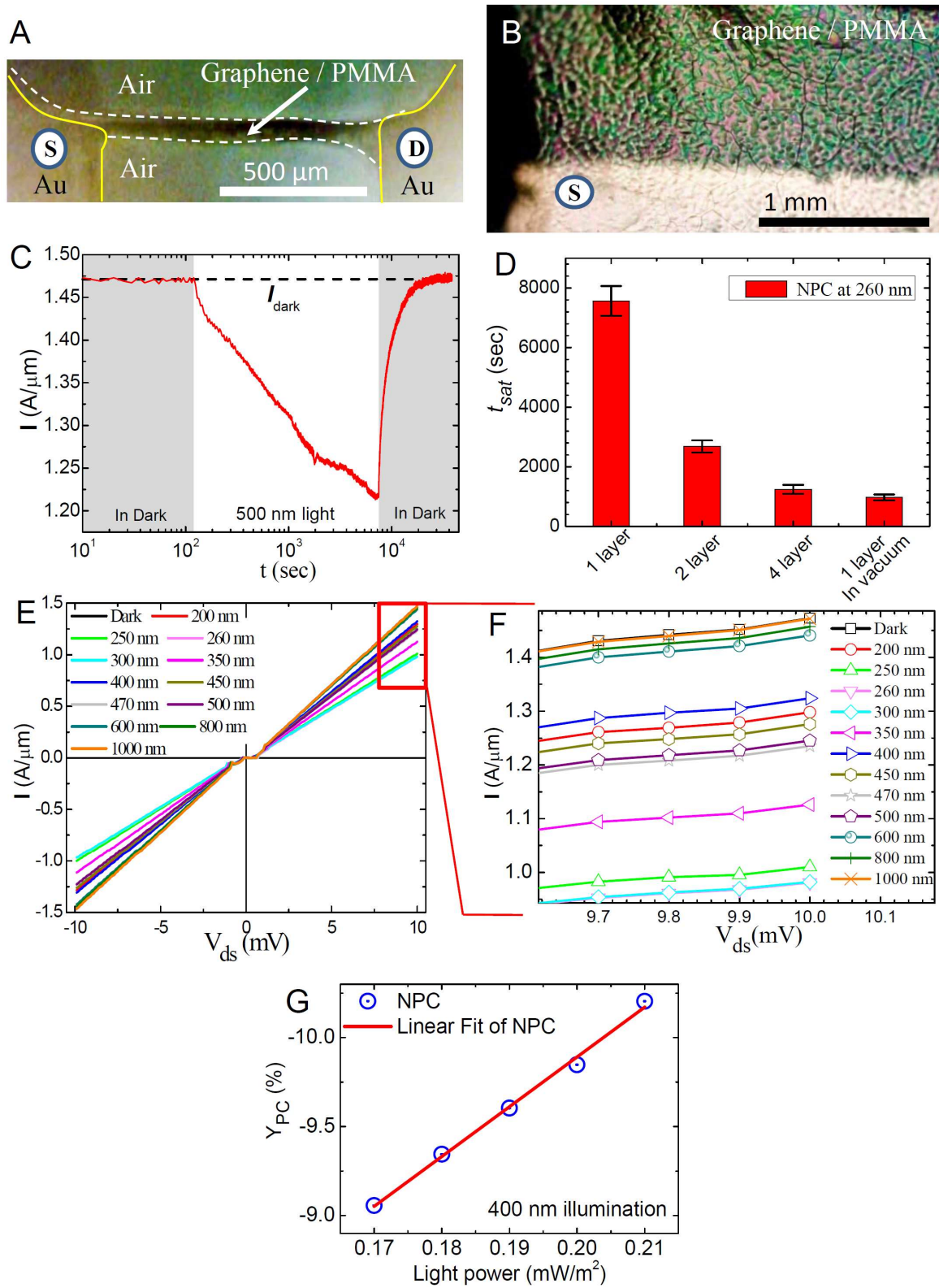
A Air
Graphene / PMMA
Air
S Au
D Au
500 μm

B Graphene / PMMA
S
1 mm

C
In Dark
I_{dark}
500 nm light
In Dark

I (A/μm)
t (sec)

D
NPC at 260 nm
t_{sat} (sec)

1 layer | 2 layer | 4 layer | 1 layer In vacuum

E
Dark	200 nm
250 nm	260 nm
300 nm	350 nm
400 nm	450 nm
470 nm	500 nm
600 nm	800 nm
1000 nm	

I (A/μm)
V_{ds} (mV)

F
| Dark |
| 200 nm |
| 250 nm |
| 260 nm |
| 300 nm |
| 350 nm |
| 400 nm |
| 450 nm |
| 470 nm |
| 500 nm |
| 600 nm |
| 800 nm |
| 1000 nm |

I (A/μm)
V_{ds} (mV)

G
NPC
Linear Fit of NPC
400 nm illumination

Y_{PC} (%)
Light power (mW/m^2)

Figure S4 ǀ **(A)** Microscopic optical image (side view) of the suspended graphene device. The graphene/PMMA layer and electrodes are marked as dotted line and solid

yellow line respectively in the figure. **(B),** Optical image (top view) of the suspended graphene/PMMA layer near the source electrode. **(C)** I(t) measurements (at 10 mV bias) in monolayer of suspended graphene at 500 nm wavelength of light irradiations. **(D)** NPC saturation time (t_{sat}) comparisons of sample i, ii, iii, and iv at 260 nm irradiation. **(E)** I(V) curve at t_{sat} in sample (i) with different irradiated wavelengths. **(F)** Magnified region of graph E at the red rectangular region. **(G)** Y_{PC} variations with irradiated light power in suspended monolayer graphene device. 400 nm light wavelength was used to measure NPC yield in this case.

The relaxation of the NPC behavior after light extinguishment was also very slow process, and eventually saturates to the I_{dark} values. Light irradiation with all other wavelengths shows similar repeatable behaviors. NPC saturation time (t_{sat}) for different samples (sample i to iv) has been compared in Fig. S4D. From Fig. 2 (main text) and Fig S3, it can be understood that t_{sat} increases with increasing NPC yield. Sample (i) shows the highest t_{sat} followed by the sample (ii), (iii), and (iv). At t_{sat} condition current-voltage measurements under different irradiated wavelengths exhibits I(V) curves with different slopes (Fig. S4E), due to the sample's resistivity changes under illuminations. The magnified view of Fig. S4E (red rectangular region) shown in Fig. S4F, which clearly shows the changes in current with different irradiated wavelengths. These observations follow the similar NPC nature observed in sample (i) under fixed bias (Fig. 2B). To understand the NPC variations with irradiated photon intensity, light power was varied during NPC measurements. In the conventional photoconductors the primary photocurrent defined as $I_{ph} = (\frac{q\eta}{h\nu}) \times P_{ph}$, where q is the elementary charge, η is the quantum efficiency defined as the number of carriers generated per incident photon, P_{ph} is the incident optical power of a photon with energy $h\nu$ (*S3*). The above equation shows directly proportional relationship between incident photon power and photogenerated current. Significantly, in our investigations NPC yield ($Y_{NPC} = |I_{dark} \sim I|/I_{dark}$, the amount of change in I due to photon irradiation w. r. t. I_{dark}) in suspended graphene varies proportionally with the illuminated light power ($Y_{NPC} \propto P_{ph}$) (Fig. S4G) as observed previously in functionalized nanoparticles (*S4*).

5. Current dynamics during NPC & PPC in graphene deposited on SiO$_2$ substrate

NPC yield (Y_{NPC}) in graphene found maximum in monolayer suspended graphene (34%). However, NPC yield significantly reduced in graphene layer transferred on to arbitrary substrate, i.e. 10.5% in monolayer graphene transferred on to SiO$_2$/Si substrate, 12% in monolayer graphene transferred on to SiO$_2$/PET, and 10% in monolayer graphene transferred on to PET substrate. Among these substrates only SiO$_2$/Si substrate shows both NPC and PPC consecutively (Fig. 1, 2, S5A), highlights the presents of PPC behavior caused by the
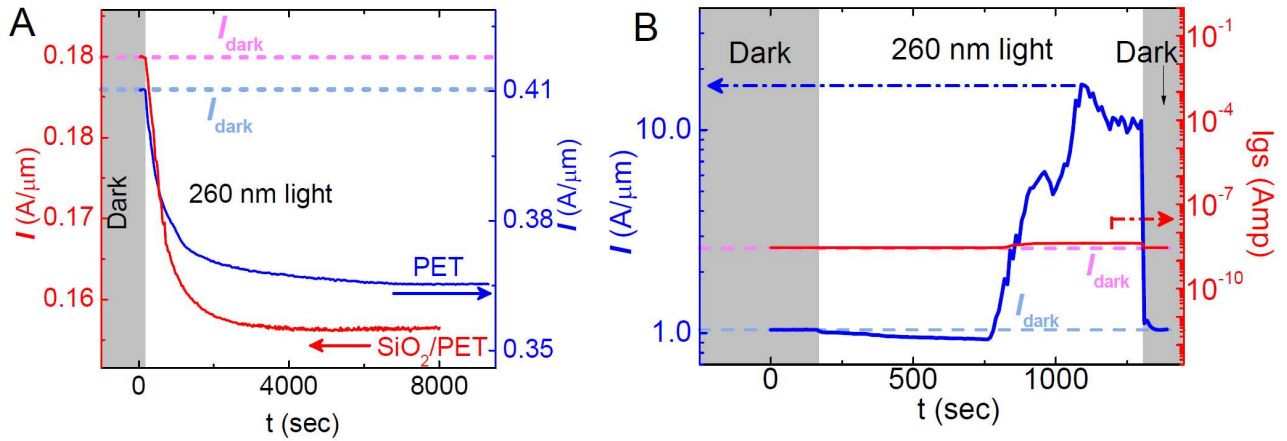

Figure S5 | **(A)** Simultaneous measurements of I$_{ds}$(t) (I$_{ds}$: source to drain current through graphene channel) and I$_{gs}$(t) (I$_{gs}$: source to gate (Si substrate) current) in dark and 260 nm light illumination. **(B)** I(t) measurements of single layer graphene transferred on to PET and SiO$_2$/PET substrate.

combination of SiO$_2$ and Si substrate effects under continuous photoexcitation. To ensure the PPC current flow to the electrodes not coming from the photoexcited Si substrate, we measured simultaneous current flow from Si substrate to the electrodes (I_{gs}) while measuring graphene photoconductance (Fig. S5B). I_{gs} current remains constant at nano ampere level with or without light illumination confirming the current flow at PPC_{satu} is not coming from the Si substrate.

6. Correlation between PPC and NPC

The PPC is exclusively observed only in graphene device transferred onto SiO_2/Si substrate along with distinct NPC behavior. However, graphene transferred onto SiO_2/PET, PET substrate including suspended graphene exhibits only NPC behavior upon light illumination. This confirms the NPC phenomenon is independent of the substrate used in this study and driven mainly by the charge scattering in graphene itself. The original graphene device is p-type due to the presence of oxygen related functional groups on the graphene surface. The localized adsorbates (oxygen/hydroxyl) related impurity states near the Fermi level increase the photogenerated charge scattering of the hole carriers, which invokes the NPC phenomenon upon light illumination. However, this NPC phenomenon is transient in nature and saturates (minimum NPC) in a long time scale of few hours (Fig. 2b) depending on the fraction of adsorbates scattering compared to carrier conduction in graphene. In contrast, PPC is substrate-dependent phenomenon and correlated with the reduction of the charge impurities in the substrate. The occurrence of PPC effect in graphene transferred onto a SiO_2/Si substrate is triggered much earlier than the saturation of NPC due to significant reduction of charge impurities of graphene/SiO_2 and SiO_2/Si interfaces by continuous photogenerations in Si substrate (Fig. 1a). Therefore, maximum PPC value depends directly on the maximum annihilation of the charge impurities present at the oxide layers and its interfaces and independent of minimum values of NPC in graphene layers.

7. Changes in density of states by adsorbed absorbents on graphene surface

We theoretically calculated the electronic density of states (DOS) and partial density of states (PDOS) of graphene (containing 24 carbon atoms) with oxygen (Fig. 4B), hydroxyl (OH) (Fig.
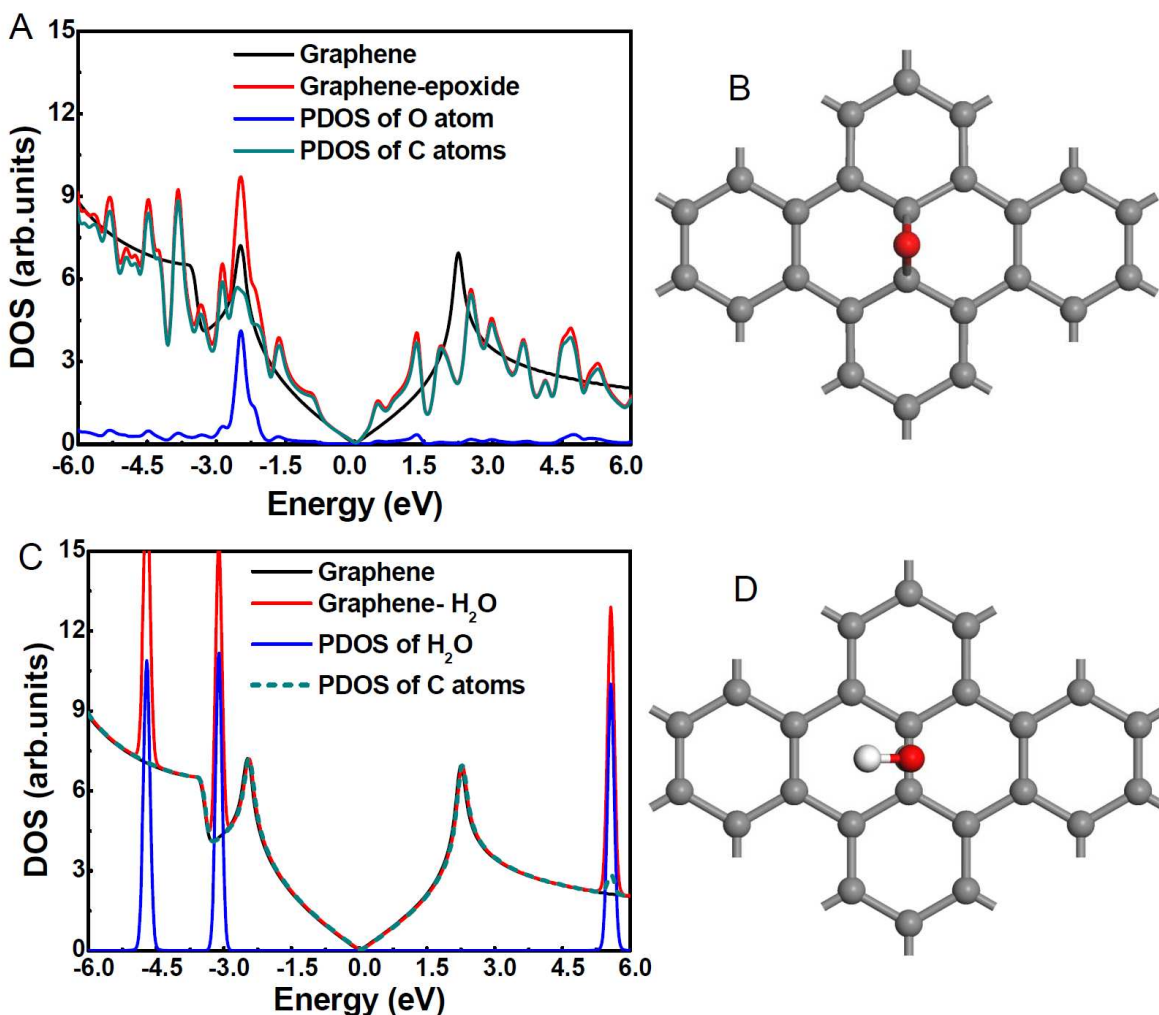

Figure S6 ǀ (A-D) GGA calculation of electronic density of states (DOS), and partial density of states (PDOS) of pure graphene monolayer (containing 24 carbon atoms per unit cell), with oxygen atom (A), water (C) doped [one oxygen (B), hydroxyl (D) molecule attached per unit cell] graphene monolayer. Fermi level of graphene is located at zero eV energy.

4C), oxygen atom (Fig. S6A), and water (Fig. S6C) absorbents on graphene surface. Fig. S6B and Fig. S6D represents the top view of oxygen atom and water molecule attachment with

carbon atoms. Fermi level is located at zero energy. Significantly, only oxygen and OH absorbents shows large localized states at the Fermi level of graphene (Fig. 4B, C) whereas, oxygen atom and water absorbents do not show such behavior near the Fermi level (Fig. S6A, C). Graphene-epoxide shows fluctuations in the DOS (except Fermi level regions) with respect to pristine graphene DOS. However, there is no localized state found near to the Fermi level of graphene due to epoxide incorporation. Graphene-water DOS does not differ significantly with respect to pristine graphene case except the energy region of water PDOS. In this case there is no localized state found near to the Fermi level of graphene also.

References:

S1.   Nair, R. R. *et al.* Fine Structure Constant Defines Visual Transparency of Graphene. *Science* **320,** 1380 (2008).

S2.   Ferrari, A. C. *et al.* Raman Spectrum of Graphene and Graphene Layers. *Phys. Rev. Lett.* **97,** 187401 (2006).

S3.   S. M. Sze, *Physics of Semiconductor Devices* (Wiley, New York, ed. 2, 1981).

S4.   H. Nakanishi *et al., Nature* **460,** 371-375 (2009).